Geofísica Internacional (2024) **63-2**: 865 - 879

Investigation of Salanda Fault Zone, between Yesiloz and Gumuskent (Nevsehir-Turkey) with PSInSAR

Ramazan Demircioğlu[*1] and Osman Oktar[2]

Abstract

In this study, the section of the Salanda fault zone between Yesiloz village and Gumuskent (Nevsehir, Turkey) was investigated by geodetic methods, and the amount of movement in this area was determined. We used a Persistent Scatterer Interferometric Synthetic Aperture Radar (PSInSAR) to determine the line of sight (LOS) movement. Previous studies using geological and geomorphological indices have shown that the Salanda fault zone is active. For the first time in this study, 36 synthetic aperture radar (SAR) images acquired between January 8, 2020, and November 29, 2022, were used in PSInSAR analysis. When the annual velocity values of the stud area in the LOS direction were analysed, annual subsidence values of up to 7.6 mm and annual uplift values of up to 7.2 mm were revealed. These movements indicate that the Salanda fault is active and normal fault characteristics. However, it also has a dextral strike-slip component.

Key words: Central Anatolia, active tectonics, Salanda fault zone, GNSS, PSInSAR.

Resumen

En este estudio, se investigó la sección de la zona de la falla de Salanda entre el pueblode Yesiloz y Gumuskent (Nevsehir, Turquía) mediante métodos geodésicos, y sedeterminó la cantidad de movimiento en esta zona. En este estudio, con este fin utilizamosun radar de apertura sintética interferométrico de dispersión persistente (PSInSAR) paradeterminar el movimiento de la línea de visión (LOS). Estudios anteriores realizados conínndices geológicos y geomorfológicos han demostrado que la zona de la falla de Salandaestá activa. Por primera vez en este estudio, se utilizaron en el análisis PSInSAR 36imágenes de radar de apertura sintética (SAR) adquiridas entre el 8 de enero de 2020 y el29 de noviembre de 2022. Cuando se analizaron los valores anuales de velocidad delárea de estudio en la dirección LOS, se revelaron valores anuales de subsidencia dehasta 7,6 mm y valores anuales de elevación de hasta 7,2 mm. Estos movimientosindican que la falla de es activa y tiene características de falla normal. Sin embargo,también tiene un componente de deslizamiento dextral.

Palabras clave: Anatolia Central, tectónica activa, zona de falla de Salanda, GNSS, PSInSAR.

Received: August 2, 2023; Accepted: January 9, 2024; Published on-line: April 1, 2024.

Editorial responsibility: Dr. Rakesh Dumka

* Corresponding author: Ramazan Demircioğlu. E-mail: ra.demircioglu@gmail.com
[1] Department of Emergency Aid and Disaster Management, Aksaray University, Aksaray, Turkey.
[2] Department of Geomatics Engineering, Aksaray University, Aksaray, Turkey. osman.oktar38@gmail.com

https://doi.org/10.22201/igeof.2954436xe.2024.63.2.1733

1. Introduction

The study area is located on the Kırşehir Block, one of the tectonic units of Turkey, approximately in the middle of Turkey and north of Nevşehir Province (Figure 1).

Palaeozoic to Quaternary age rocks are found in and around the study area, as shown in Figure 2. The basement of the study area is made up of Palaeozoic-Mesozoic metamorphic rocks from the Kırşehir Massif, which are cut by Late Cretaceous igneous rocks. These units are unconformably overlain by Palaeocene-Middle Eocene sedimentary units known as the Ayhan Group. Additionally, Middle Miocene-Quaternary units unconformably overlap these units. Polyphase deformation has occurred in the basement metamorphic rocks in the study area.

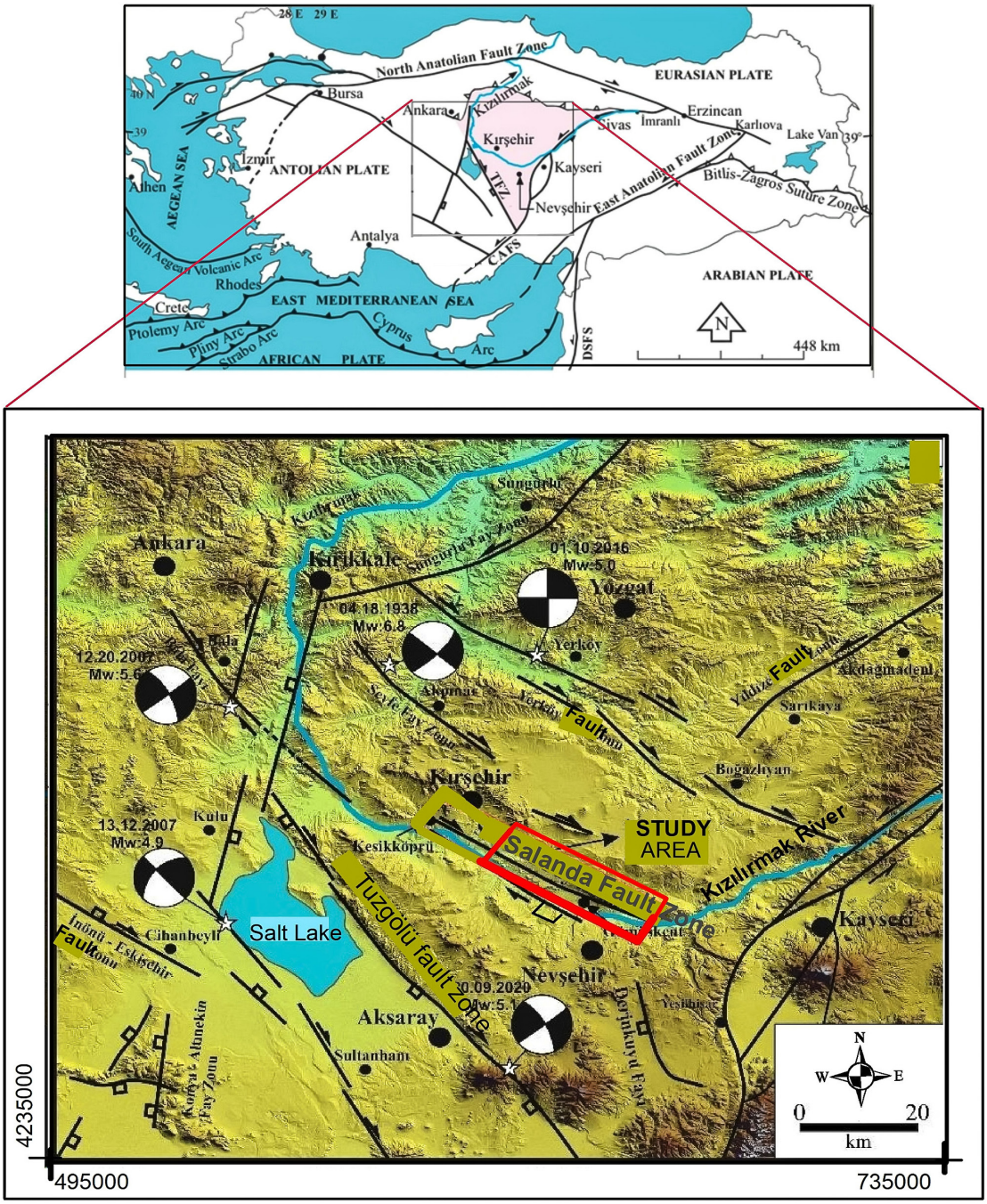

Figure 1. The study area location map.

Palaeozoic to Quaternary age rocks are found in and around the study area, as shown in Figure 2. The basement of the study area is made up of Palaeozoic-Mesozoic metamorphic rocks from the Kırşehir Massif, which are cut by Late Cretaceous igneous rocks. These units are unconformably overlain by Palaeocene-Middle Eocene sedimentary units known as the Ayhan Group. Additionally, Middle Miocene-Quaternary units unconformably overlie these units. Polyphase deformation has occurred in the basement metamorphic rocks in the study area. Palaeozoic to Quaternary age rocks are found in and around the study area, as shown in Figure 2.

The basement of the study area is made up of Palaeozoic-Mesozoic metamorphic rocks from the Kırşehir Massif, which are cut by Late Cretaceous igneous rocks. These units are unconformably overlain by Palaeocene-Middle Eocene sedimentary units known as the Ayhan Group. Additionally, Middle Miocene-Quaternary units unconformably overlie these units. Polyphase deformation has occurred in the basement metamorphic rocks in the study area. Due to the closure of the Inner Tauride Ocean, the basement units and the rocks of the Ayhan Group underwent polyphase deformation. The Palaeocene-Middle Eocene units unconformably overlying these basement units have undergone at least 3 stages of folding. In the study area, the extensional tectonic regime began in the Late Miocene according to field studies (Demircioglu, 2014).

In the Middle Miocene units, folds were formed due to a compressional tectonic regime. However, in the units formed after the Late Miocene-Pliocene period, no structures belonging to the compressional tectonic regime were observed. Instead, normal faults were formed due to the influence of the extensional regime.

In the study area, northeast-southwest-trending normal faults were formed due to the northeast-southwest-trending extensional tectonic regime. The most significant fault in this area is the Salanda fault zone, which consists of several segments. In this study, we analyzed the movements of this fault between Yesilöz and Gumuskent using the PSInSAR method. According to the studies of Şengör and Yılmaz (1981), the Salanda fault zone, which is the subject of this study, is located in the Central Anatolian Plain region. Central Anatolia was under an extensional tectonic regime during the Neotectonic Period (Şengör and Yılmaz (1981), Koçyiğit (1984, 2003). The resulting faults generally developed as normal and extensional strike-slip faults. Koçyiğit and Doğan (2016) conducted a study on the neotectonic faults of Central Anatolia (Figure 3).

The study area is located in the Central Anatolian region, east of the Tuzgölü fault zone and north of Nevşehir province (Figure 3). One of the most important fault zones in Central Anatolia in Turkey is the Salanda fault zone. A satellite-based study on this fault zone has been carried out for the first time in this study.

This study aims to investigate the characteristics of the Salanda fault zone between Yesiloz-Gumuskent in the study area. For this purpose, field and PSInSAR studies were carried out.

The Salanda fault, which is the focus of this study, is one of the normal faults that developed in Central Anatolia during

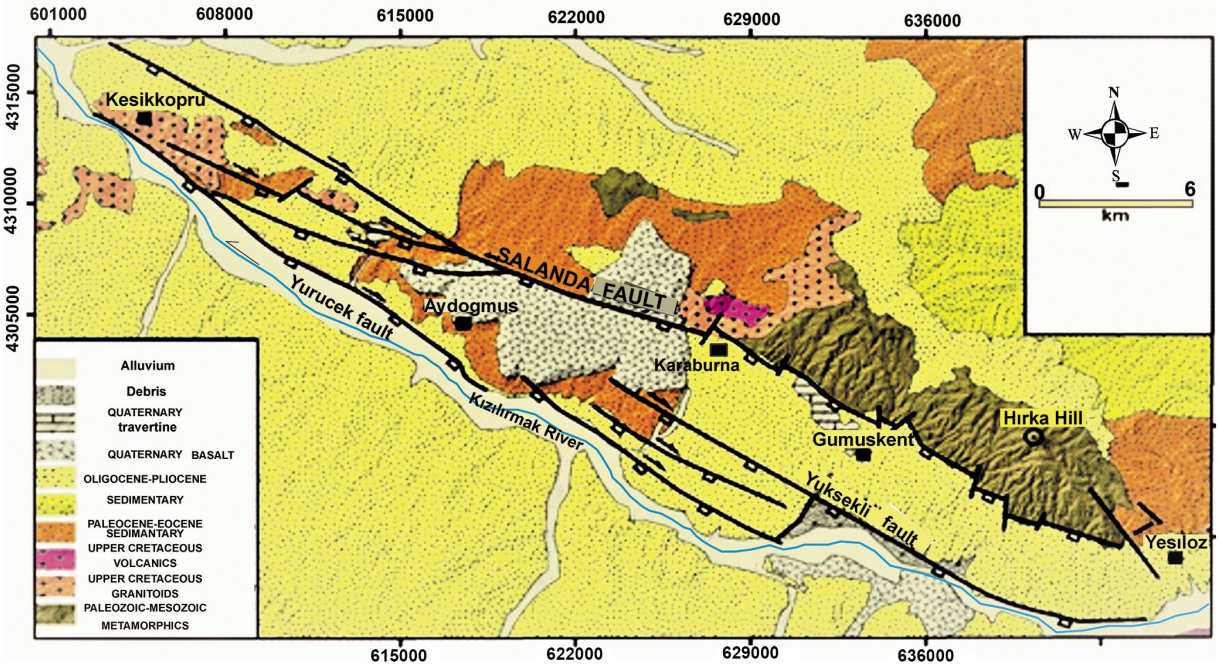

Figure 2. Geological map of the study area and the Salanda Fault (Modified from Demircioğlu and Coşkuner, 2022)..

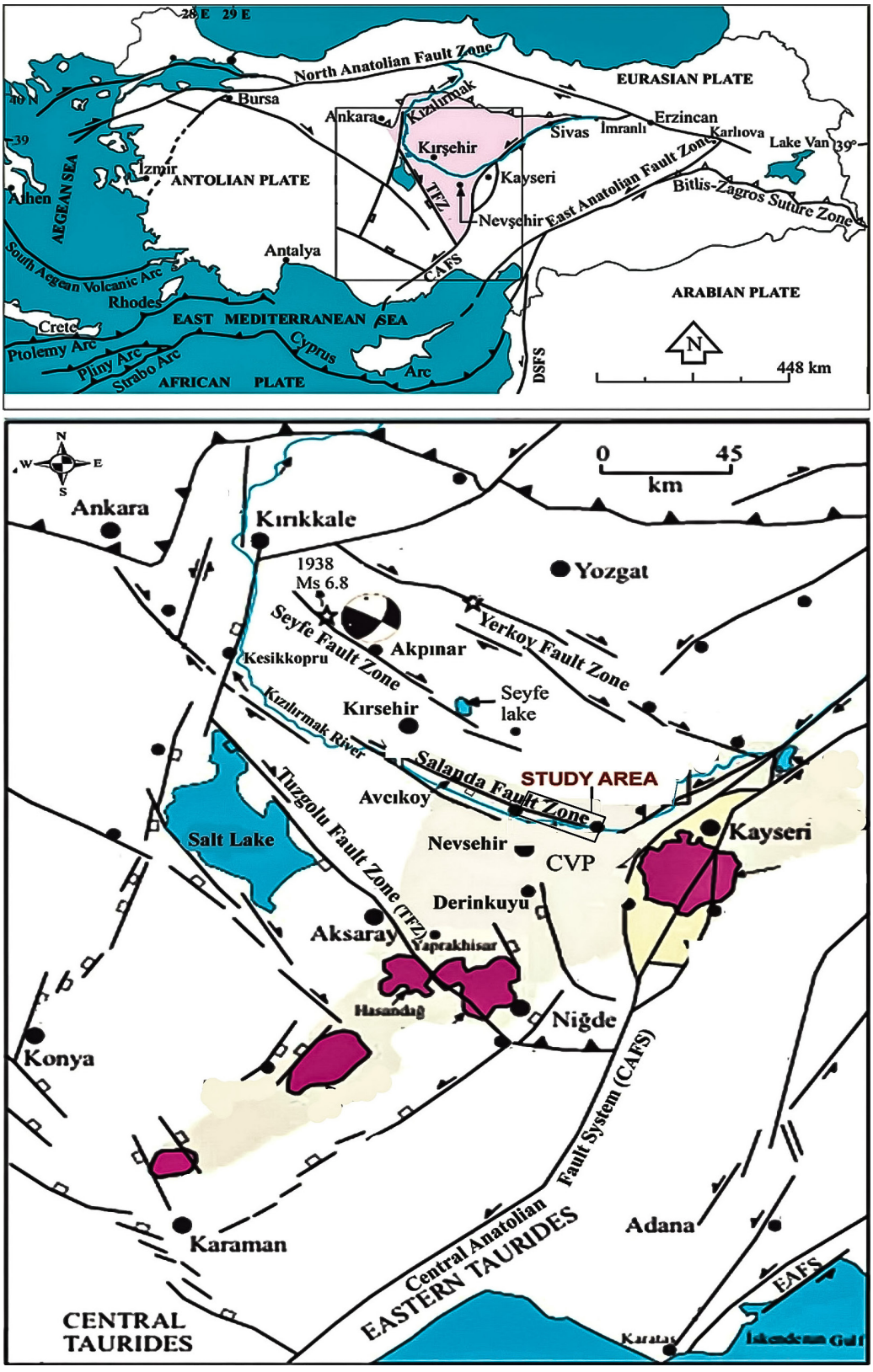

Figure 3. Simplified map showing plate tectonics and neotectonic faults of Turkey. CVP: Central Anatolian Volcanic Province (Modified from Koçyiğit and Doğan, 2016).

the Neotectonic period. This development was due to the northeast-southwest extensional tectonic regime. The Yerköy, Seyfe, Salanda, and Tuzgolu faults are examples of such normal faults, which also have lateral thrusts. The extensional tectonic regime created fault directions that run in a northwest-southeast direction, as shown in Figure 3.

The study area has Palaeozoic-Mesozoic age metamorphic rocks belonging to the Kırşehir Massif, and Late Cretaceous age igneous rocks cut these rocks. Palaeocene-Quaternary rocks unconformably overlie these units. The Salanda fault zone has travertines formed by it. Additionally, the fault cut the Quaternary basalts. These deformations are visible in the field, as shown in Figure 2. The Salanda fault, which is the focus of this study, is one of the normal faults that developed in Central Anatolia during the Neotectonic period. This development was due to the northeast-southwest extensional tectonic regime. The Yerköy, Seyfe, Salanda, and Tuzgolu faults are examples of such normal faults, which also have lateral thrusts. The extensional tectonic regime created fault directions that run in a northwest-southeast direction, as shown in Figure 3.

The study area has Palaeozoic-Mesozoic age metamorphic rocks belonging to the Kırşehir Massif, and Late Cretaceous age igneous rocks cut these rocks. Palaeocene-Quaternary rocks unconformably overlie these units. The Salanda fault zone has travertines formed by it. Additionally, the fault cut the Quaternary basalts. These deformations are visible in the field, as shown in Figure 2. The Salanda fault, which is the focus of this study, is one of the normal faults that developed in Central Anatolia during the Neotectonic period. This development was due to the northeast-southwest extensional tectonic regime. The Yerköy, Seyfe, Salanda, and Tuzgolu faults are examples of such normal faults, which also have lateral thrusts. The extensional tectonic regime created fault directions that run in a northwest-southeast direction, as shown in Figure 3.

The study area has Palaeozoic-Mesozoic age metamorphic rocks belonging to the Kırşehir Massif, and Late Cretaceous age igneous rocks cut these rocks. Palaeocene-Quaternary rocks unconformably overlie these units. The Salanda fault zone has travertines formed by it. Additionally, the fault cut the Quaternary basalts. These deformations are visible in the field, as shown in Figure 2. The Salanda fault, which is the focus of this study, is one of the normal faults that developed in Central Anatolia during the Neotectonic period. This development was due to the northeast-southwest extensional tectonic regime. The Yerköy, Seyfe, Salanda, and Tuzgolu faults are examples of such normal faults, which also have lateral thrusts. The extensional tectonic regime created fault directions that run in a northwest-southeast direction, as shown in Figure 3.

The study area has Palaeozoic-Mesozoic age metamorphic rocks belonging to the Kırşehir Massif, and Late Cretaceous age igneous rocks cut these rocks. Palaeocene-Quaternary rocks unconformably overlie these units. The Salanda fault zone has travertines formed by it. Additionally, the fault cut the Quaternary basalts. These deformations are visible in the field, as shown in Figure 2.The Salanda fault, which is the focus of this study, is one of the normal faults that developed in Central Anatolia during the Neotectonic period. This development was due to the northeast-southwest extensional tectonic regime. The Yerköy, Seyfe, Salanda, and Tuzgolu faults are examples of such normal faults, which also have lateral thrusts. The extensional tectonic regime created fault directions that run in a northwest-southeast direction, as shown in Figure 3.

The study area has Palaeozoic-Mesozoic age metamorphic rocks belonging to the Kırşehir Massif, and Late Cretaceous age igneous rocks cut these rocks. Palaeocene-Quaternary rocks unconformably overlie these units. The Salanda fault zone has travertines formed by it. Additionally, the fault cut the Quaternary basalts. These deformations are visible in the field, as shown in Figure 2. The Salanda fault, which is the focus of this study, is one of the normal faults that developed in Central Anatolia during the Neotectonic period. This development was due to the northeast-southwest extensional tectonic regime. The Yerköy, Seyfe, Salanda, and Tuzgolu faults are examples of such normal faults, which also have lateral thrusts. The extensional tectonic regime created fault directions that run in a northwest-southeast direction, as shown in Figure 3.

The study area has Palaeozoic-Mesozoic age metamorphic rocks belonging to the Kırşehir Massif, and Late Cretaceous age igneous rocks cut these rocks. Palaeocene-Quaternary rocks unconformably overlie these units. The Salanda fault zone has travertines formed by it. Additionally, the fault cut the Quaternary basalts. These deformations are visible in the field, as shown in Figure 2. Using the Persistent Scatterer Interferometric Synthetic Aperture Radar (PSInSAR) technique, surface deformation can be easily monitored spatially (Poyraz and Hastaoğlu 2020). PSInSAR is a widely used geodetic method that has been applied in recent years. The PSInSAR method has been widely used in deformation-observing scientific research focusing on tectonic movements (Arıkan *et al.* 2010; Poyraz and Hastaoğlu 2020; Dumka *et al.* 2020; Dumka *et al.* 2021; Suribabu *et al.* 2022a; Suribabu *et al.* 2022b; Dumka *et al.* 2023), in the determination of earthquake-induced surface movements (Yen *et al.* 2011; Suárez *et al.*, 2018; Famiglietti, 2022), landslide monitoring (Peyret *et al.* 2008; Hastaoğlu *et al.* 2014), volcanic (Hooper *et al.* 2004, 2007; Gündüz *et al.* 2023), geological and urban areas (Meisina *et al.* 2006; Rodríguez *et al.*, 2012; Gezgin 2022; Dumka *et al.* 2022), and subsidence in mining areas (Abdikan *et al.* 2014).

This study aims to determine the tectonic movements and surface deformations in the Salanda Fault Zone. To this end, PSInSAR was applied to the Salanda Fault Zone to determine movements in the line of sight (LOS) of the area. The PSInSAR analyses were performed using the Stanford Method for Persistent Scatterers (StaMPS)/MIT software (Hooper *et al.* 2018). The novelty of this study is the lack of any geodetic study related to the Salanda fault. The results of our study are important in that the velocity information obtained from the analysis results can be used by different disciplines, such as geology and geophysics.

1.1 Salanda Fault Zone

In the study area, the neotectonic period started during the Late Miocene-Early Pliocene (Demircioglu, 2014). Following this period, the study area and its surroundings were affected by the extensional tectonic regime which led to the formation of

normal faults. Even though these faults have strike-slip movements, they exhibit normal faulting characteristics. The strike-slip faults observed in and around the study area indicate that they were formed under the extensional tectonic regime.

The Salanda fault zone was first identified in the study of Koçyiğit (1984), and it has been determined that the length of the fault is 60 km. The Salanda fault has different segments, and its strikes vary between N40-800E and N450W-N820W. The dip of the fault plane is observed towards the southwest and southeast with values ranging from 58 to 72 degrees (as shown in Figures 2, 3, and 4). One of the best places to observe the fault is southeast of Gumuskent (Figure 5).

In the following years, studies were carried out on the Salanda Fault (Şaroğlu *et al.*, 1987; Atabey, 1989). Şaroğlu *et al.* (1987) mentioned in their study that the Salanda fault zone cuts the Quaternary units and causes deformation in them. Therefore, they considered the Salanda fault as an active fault. Doğan (2011) obtained Quaternary (1.9 my. to 96 ka) ages in his radiometric dating of the basalts observed in the study area. In the north of the field, it was observed during field studies that the Quaternary

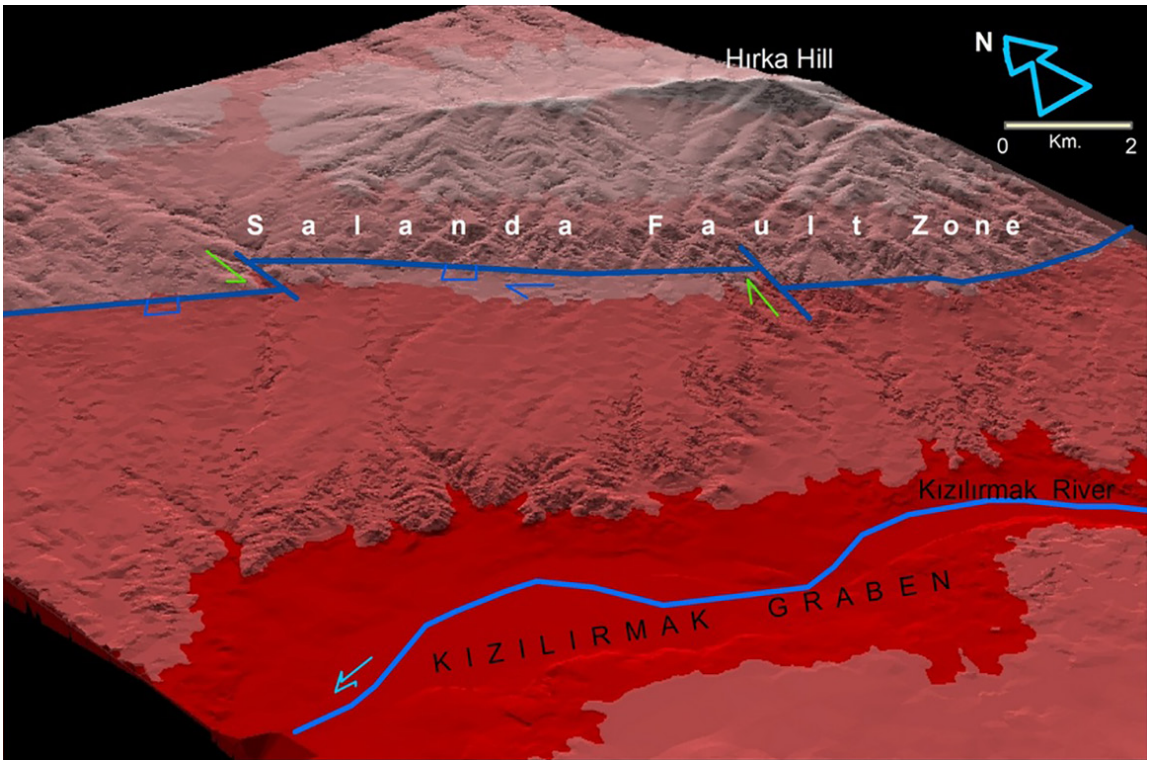

Figure 4. The Salanda fault zone and the Kızılırmak Graben (Between Yesıloz-Gumuskent village).

Figure 5. View of the Salanda fault zone from southeast of Gumuskent (Gumuskent-Yesıloz road).

basalts around Karaburna were cut by the Salanda fault. Temiz (2004) and Temiz *et al.* (2009) found 70145-96080 years (late Pleistocene) and 18040-8700 years old (late Pleistocene-Holocene) by uranium ageing method on travertines in the vicinity of Avcıkoy, northwest of the study area.

In Turkey, the neo-tectonic onset of each region is different. In the study area, the neo-tectonic period begins in the Late Miocene-Lower Pliocene (Demircioğlu, 2014). After this period, Central Anatolia came under an extensional tectonic regime. There are important faults in and around the study area. During the instrumental period, catastrophic earthquakes occurred on these faults (Figure 6).

In 1938, a magnitude 6.8 earthquake occurred on the Akpınar fault, which is the continuation of the Salanda fault (Figures 3, 6).

Non-instrumental period earthquakes are said to have occurred among the people. Demircioğlu and Coşkuner (2022) found that the fault showed medium-high tectonic activity in the geomorphic index studies of the Salanda fault zone between Yeşilöz and Kesikköprü. In the study of Koçyiğit and Doğan (2016), the annual right lateral offset was 4 mm since the Pleistocene, and they determined the length of the fault to be 66 km.

Along the Kızılırmak valley, where the Salanda Fault borders on one side, there are some studies on the fault (Koçyiğit, (2003), Doğan *et al.*, (2009), Doğan, (2011), Çiner *et al.*, (2015). In addition, with the development of satellite and measurement technologies in recent years, studies to determine the amount of movement on fault lines have intensified (Biggs *et al.*, 2007; Yavaşoğlu *et al.*, 2011; Shirzaei and Bürgmann 2013; Wang and Johnson 2015; Rosu *et al.*, 2015; He *et al.*, 2019; Gürsoy *et al.*, 2017; Liu and Zhao, 2020; Scott *et al.*, 2020; Peterson *et al.*, 2020; Howel *et al.*, 2020).

The Salanda fault zone is located in the northeastern part of the Kızılırmak graben, through which the Kızılırmak River flows. This is one of the faults that played an important role in the formation of the graben.

2. Materials and Methods

Geological and geomatic studies carried out in the area were evaluated together and new data on the Salanda fault zone were obtained. A geological map was produced from field studies in

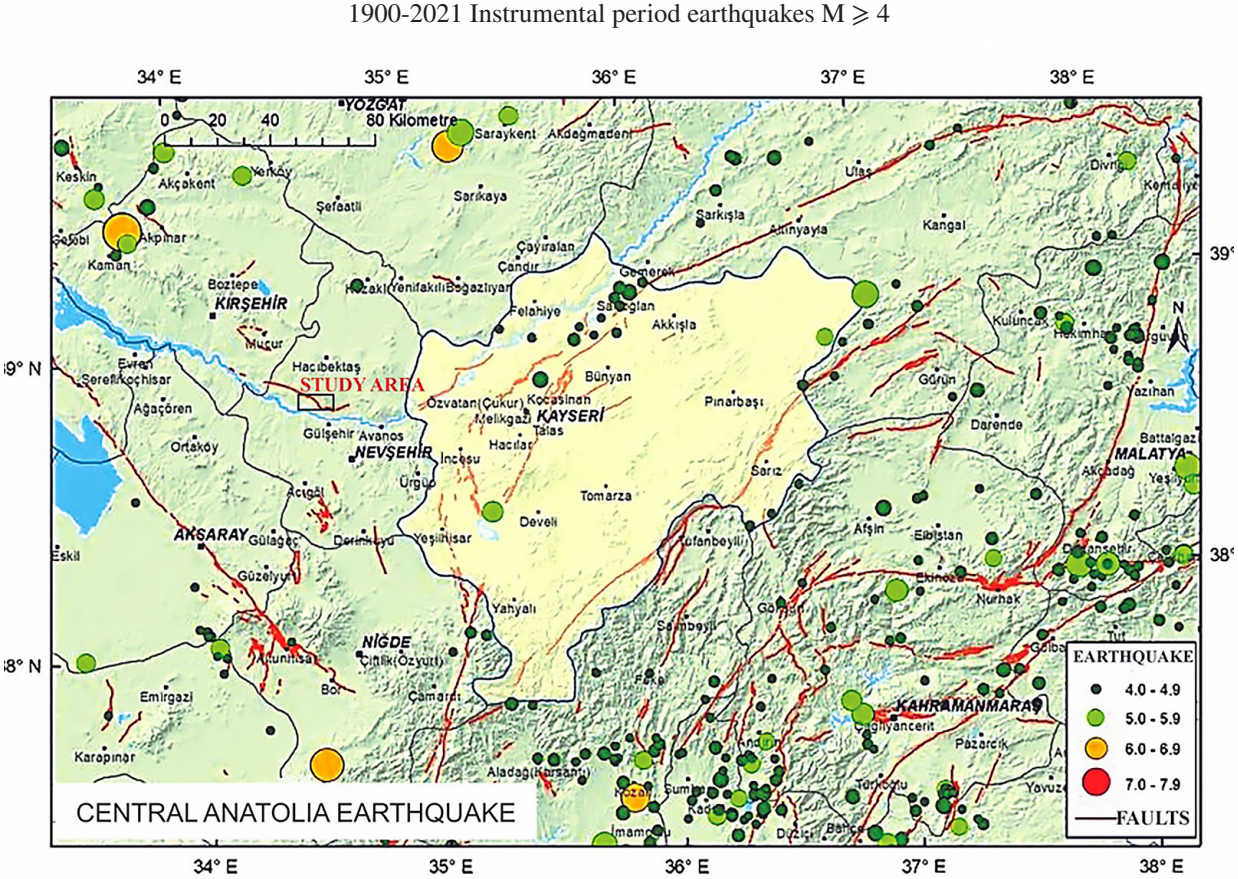

Figure 6. Earthquakes in and around the study area (Modified from Kandilli, 2022).

the area. The young units cut by the Salanda fault zone were analysed in detail. The fact that it cuts basalts that are radiometrically dated and determined to be of Quaternary age indicates that the fault is active. In addition to these field data, geomatic data were required, and 3 years of data were obtained for this area. The field and geomatics data obtained were analysed together to provide data on the extent of the fault zone's vertical and horizontal movement and activity These data were analysed using computer software. Plots of these data were produced.

2.1 Study Area Field dataset

Mapping investigations were conducted on the Salanda fault zone segments during the field survey of the research region. We spotted the young units that were severed by the fault. In the field, the fault planes' strike and dip values were measured, and the fault lines' variations were identified. Figure 6 displays the seismic data that was collected for the research region and its environs. In particular, faulting was shown to have altered the Kızılırmak River's bed.

We followed the river's ancient beds. Geological information was gathered on the degree of displacement, which was previously ascertained by other studies.Seismic activities are observed in and around the Salanda fault.

2.3 PSInSAR data acquisition

Images from the European Space Agency's Sentinel-1 satellite were used in the PSInSAR analysis. The data of the Sentinel-1A synthetic aperture radar (SAR) images are shown in Table 1.

The total SAR coverage (Track 14) is shown in Figure 7. In addition, these data have been added to the Google Earth image.

Table 1. Dates of the SAR images used.

Sentinel-1A		
2020.01.08	2021.01.02	2022.01.09
2020.02.01	2021.02.07	2022.02.02
2020.03.08	2021.03.03	2022.03.10
2020.04.01	2021.04.08	2022.04.03
2020.05.07	2021.05.02	2022.05.09
2020.06.12	2021.06.07	2022.06.02
2020.07.06	2021.07.01	2022.07.20
2020.08.11	2021.08.06	2022.08.01
2020.09.04	2021.09.11	2022.09.06
2020.10.10	2021.10.05	2022.10.12
2020.11.03	2021.11.10	2022.11.05
2020.12.09	2021.12.04	2022.11.29

This image shows the uplift and subsidence zones caused by the Salanda fault zone (Figure 8). The approximate boundaries of the uplift and subsidence zones also form fault lines.

36 Sentinel-1 SAR images have been used in this study. The SAR images are interferometric wide (IW), C-band, track number 14, and were acquired between 08.01.2020 and 29.11.2022. The Copernicus Open Access Hub (URL-1) provided the SAR images free of charge.

2.2 PSInSAR analysis

The StaMPS software has been developed to analyse movement over the continent (Hooper *et al.* 2007). In addition, the PSInSAR technique has been applied, which brings a different approach. These methods use the spatial correlation of the interferometric phase to find pixels with low phase change. This makes it possible to analyse all types of terrain, excluding man-made objects. Fixed target points are determined using adaptation maps of the interferograms. The most basic technique in the evaluation is the determination of the correlation threshold. If a target gives a higher correlation value than the mean, it is designated as a permanent scatterer (PS) point. PSInSAR analyses with a minimum of 12 SAR images are suggested to increase the number of PS points (Hooper *et al.* 2007). The time series is generated from the amplitude values of the pixels in each image. Multiple sets of interferograms are generated to identify highly fitted targets. A single master image is used to produce a set of differential interferograms for this target. When producing interferograms, it is suggested that a DEM be used to remove the effects of topography.

3. Results

3.1 PSInSAR analysis

The process consists of three main steps: interferogram generation, PS selection, and atmospheric filtration. First, appropriate sub-swath and bursts are selected in the SAR dataset, and precise orbit files are applied to them. Then, the master image is selected considering the time interval, vertical baseline, and least atmospheric effect, and all dependent images are recorded using the master image with the help of the S-1 Back Geocoding operator. After the coregistration process, interferograms are produced and prepared for StaMPS analysis by removing the topographic phase component. The entire processing block has been performed using SNAP. The next steps of the processing block are performed in the StaMPS software, and in the first step, PS candidates are selected based on the amplitude distribution

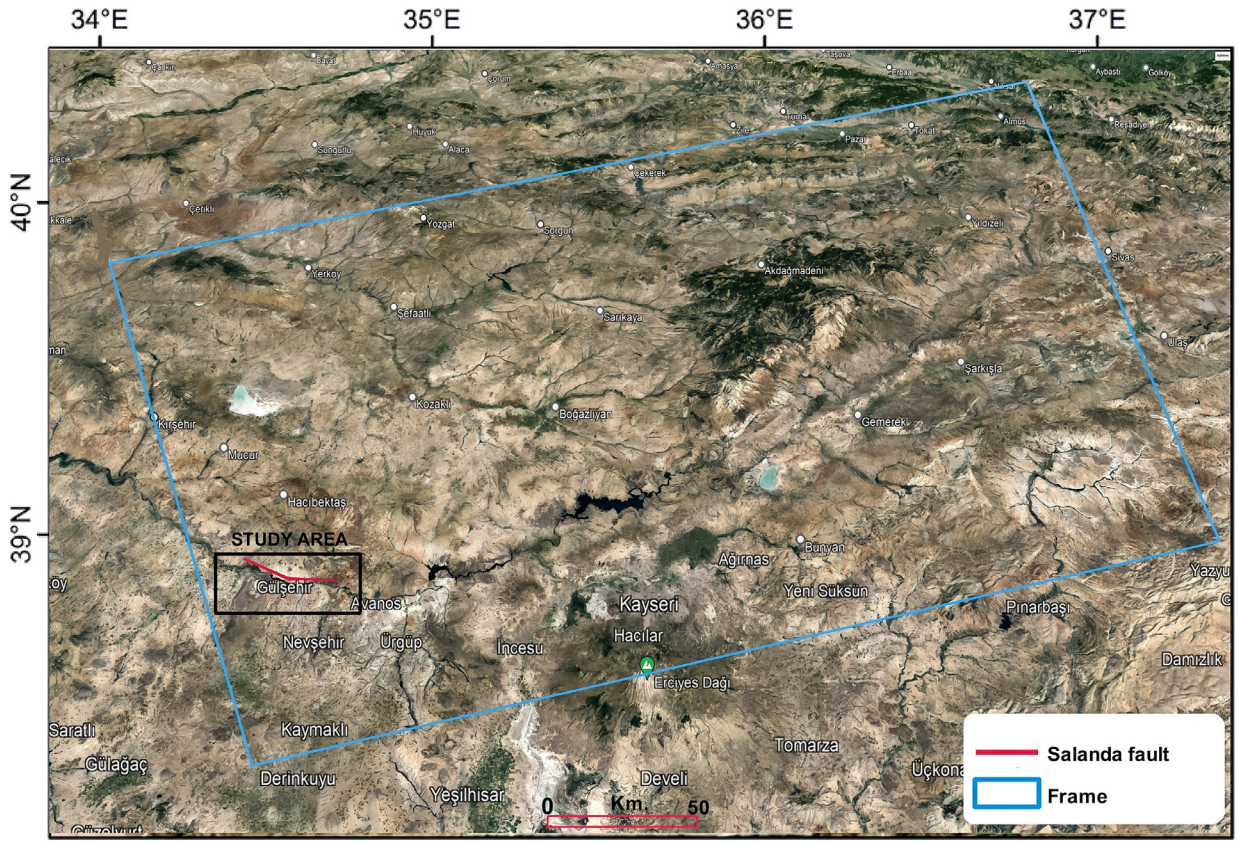

Figure 7. The blue box indicates the approximate coverage of the Sentinel-1A satellite radar images, track number 14. The red line represents the Salanda Fault (Emre *et al.* 2013).

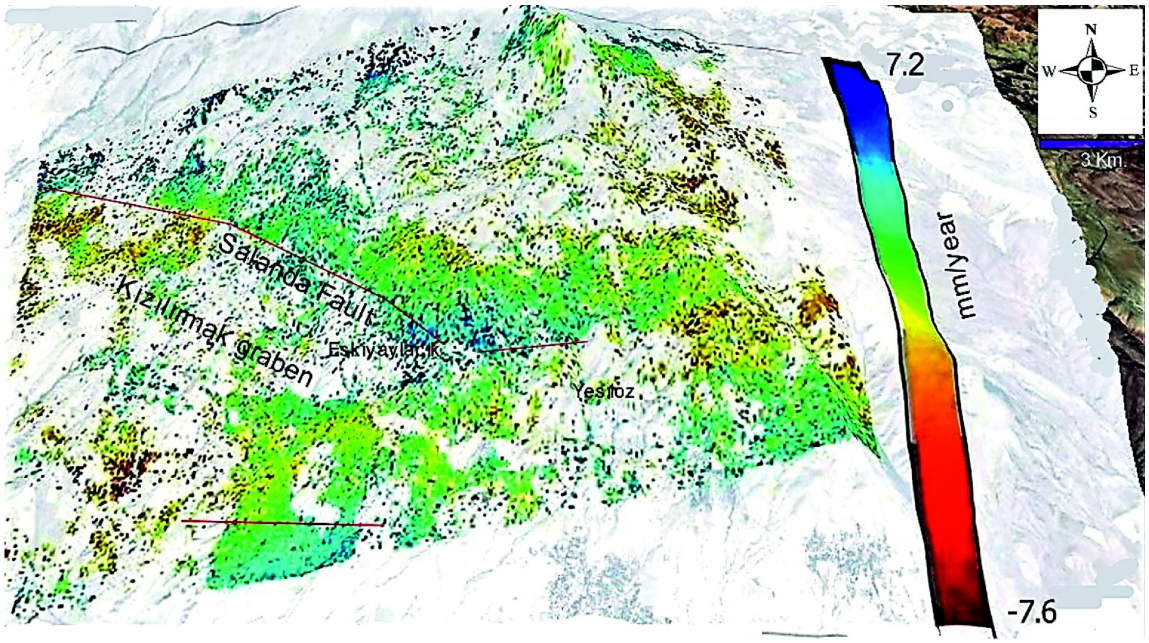

Figure 8. PSInSAR results of the study area with Google Earth image and Salanda fault.

index. The amplitude distribution index is defined as the ratio of the standard deviation of each pixel to the average amplitude value and is calculated using Equation (1) (Hooper *et al.* 2007 and Ferretti *et al.* 2001):

$$D_A \frac{\sigma_A}{\mu_A}$$

where D_A defines the amplitude dispersion value and σ_A and μ_A define the standard deviation and mean of the amplitude values (Hooper *et al.* 2007). The threshold value used is typically between 0.4 and 0.42. After determining the candidate pixels according to the amplitude distribution, the phase noise is estimated and removed for each candidate pixel using phase analysis. The residual phase of the xth pixel and the ith interferogram is given by Equation (2) (Hooper *et al.* 2007):

$$\psi_{x,i}=W\{\phi_{D,x,i}+\phi_{A,x,i}+\Delta\phi_{S,x,i}+\Delta\phi_{\theta,x,i}+\phi_{N,x,i}$$

where W{·} defines the wrapping operator, $\psi_{x,i}=W\{\phi_{D,x,i}+\phi_{A,x,i}+\Delta\phi_{S,x,i}+\Delta\phi_{\theta,x,i}+\phi_{N,x,i}$, represent the general terms for phase change due to movement of the pixel in the satellite LOS direction, phase change due to atmospheric delay between satellite passes, residual phase change due to satellite orbital error, phase change due to viewpoint, and phase noise, respectively (Hooper *et al.* 2007, Lu *et al.* 2020). Then, candidate PS points are filtered according to the noise features estimated and extracted in the previous step so that PS points in the time series are determined based on the amplitude and phase analysis for each pixel in each interferogram. After filtering the PS points, the wrapped phase is corrected for spatially uncorrelated look angle (SCLA) error, and then the phase unwrapping step is performed. In the last step, SCLA errors mostly caused by digital elevation model (DEM) errors are predicted and removed, after this step atmospheric filtering is performed, and the LOS direction velocities for the region of interest are obtained (Gündüz *et al.* 2023). The processing workflow of the study is given in Figure 9.

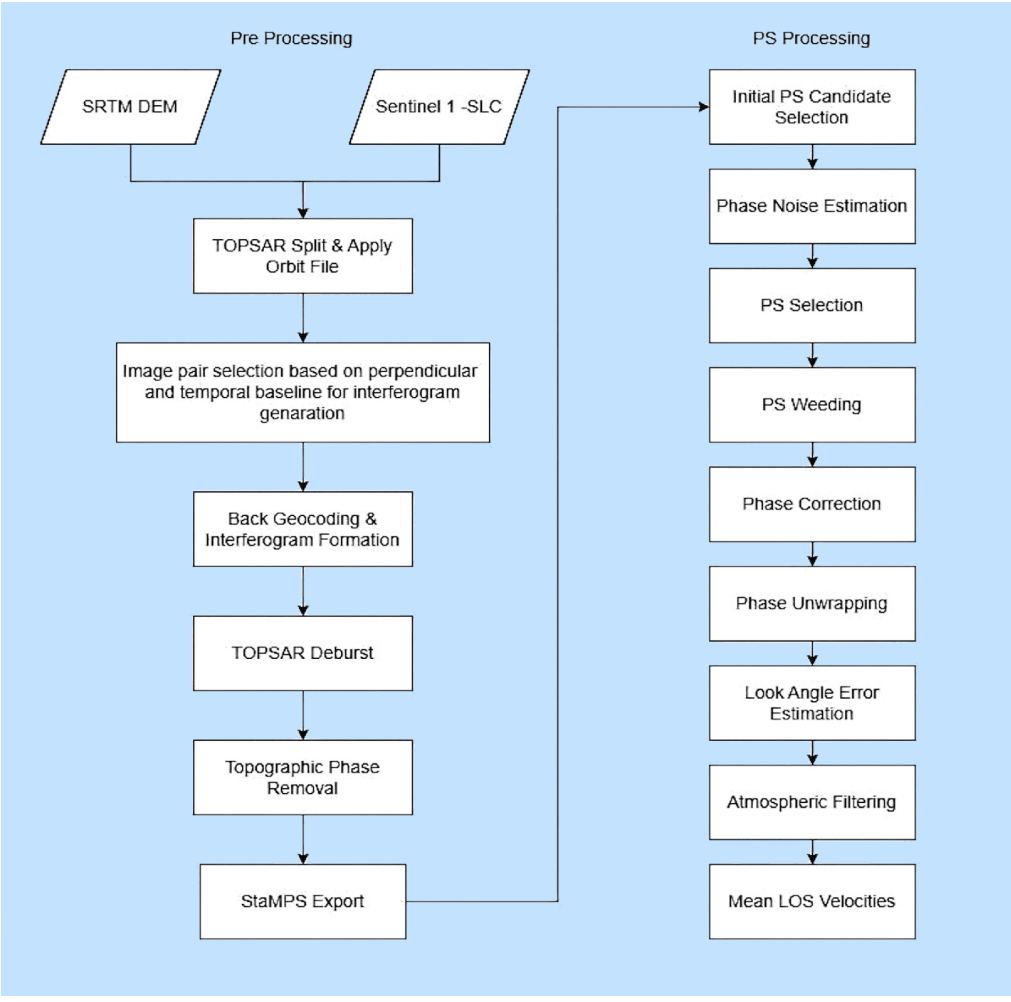

Figure 9. Processing workflow of the study.

Shuttle Radar Topography Mission (SRTM) data were used to remove the effect of topography on the interferograms. The master image was chosen to be the temporal and spatial centre of all images in the PSInSAR analysis. The 07 June 2021 image was used as the master image in the SAR image analysis. Figure 10 shows the baseline perpendicular values and the baseline temporal values with the master images.

A total of 323111 PS points were generated for the study area. The annual velocities in the study area in the LOS direction and their standard deviations are shown in Figure 11a. The vertical axis represents the latitude value while the horizontal axis represents the longitude value in Figure 11b.

In Figure 11, red indicates an uplift in the LOS direction, while blue indicates subsidence in the colour scale of the figure. The annual velocities in the study area range from -7.6 mm (lowest) to 7.2 mm (highest), while the standard deviation of the annual velocities in the LOS direction ranges from 0.4 mm to 2.7 mm (Figure 11).

4. Discussion

According to the results of the PSInSAR analysis, when the annual velocities in the LOS direction obtained for the study area are examined, annual subsidence values up to -7.6 mm and annual uplift values up to 7.2 mm were determined. Doğan *et al.* (2009), based on field observations, determined the erosion rate of the river along the Kızılırmak valley to be 0.08 mm/year during the last 2 million years. The highest rate of erosion was found to be 0.11 mm/year. In addition, Koçyiğit and Doğan (2016) determined the annual right lateral displacement as 4 mm since the Pleistocene and the length of the fault as 66 km. This study determined the average uplift values obtained from the SAR images for the last 3 years as 7.2 mm/year.

This is considerably higher than the data obtained in previous studies. According to the investigations carried out at these points along the Kızılırmak Graben, the Salanda fault zone shows high uplift values due to the normal fault character. The fault has both vertical and horizontal movement components. However, it will not be called an oblique fault as it has much less horizontal slip. According to the study of Scholz *et al.* (1987), the amount of movement and the risk of generating earthquakes, higher movement values are observed compared to intra-continental faults. It poses a risk in terms of earthquake potential. The characteristics of the segments of the Salanda fault zone are different. In particular, the larger segments should be studied in more detail, including paleoseismology.

5. Conclusions

Through the utilization of the PSInSAR methodology, this study analyzed the Salanda Fault Zone and accurately identified movements in the LOS direction. The PSInSAR data enabled a comprehensive determination of the number of movements that occurred on the Salanda Fault Zone, producing detailed information about the area with 323111 PS points. These points provided crucial insights into the magnitude of movement, field observations, and uplifts in the fault zone, particularly in areas where the fault passes, indicating significant activity. Additionally,

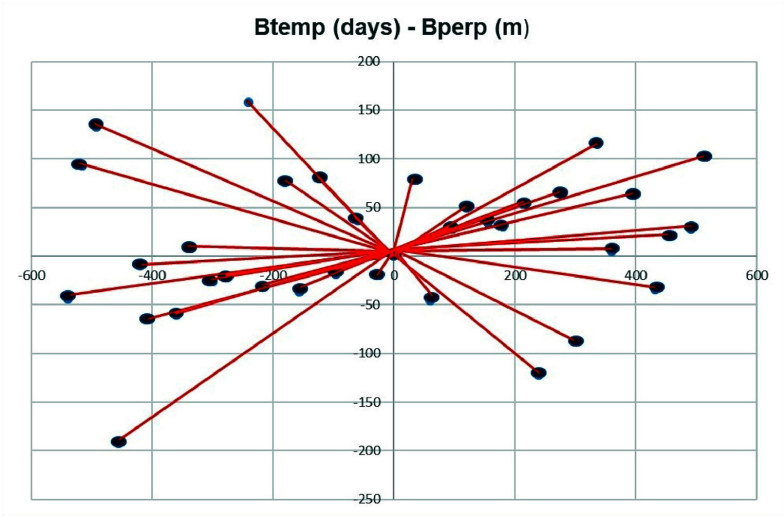

Figure 10. Temporal and spatial distribution of 36 ascending Sentinel-1 images, track number 131, based on the master image (red lines indicate interferogram pairs).

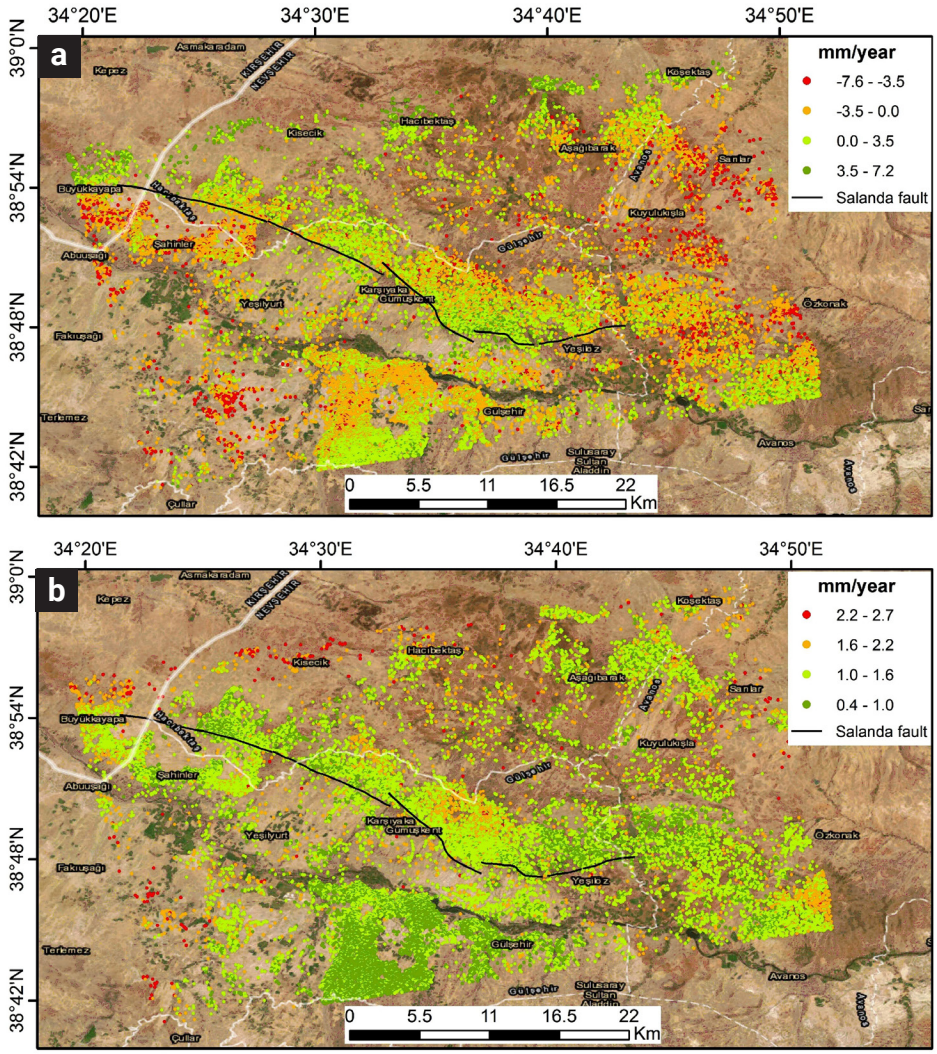

Figure 11. PSInSAR results of the study area. (a) Annual velocity in the LOS direction. (b) Standard deviations of the annual velocities in the LOS direction.

the study employed geomorphic indices (Demircioğlu and Coşkuner, 2022), revealing medium to high levels of tectonic activity.

Upon examining the historical earthquake data (Figure 6), it is evident that an earthquake measuring 6 on the magnitude scale occurred in the northwestern region of the Salanda fault zone, which is located outside of the study area. Seismic activity has been detected in and around the Salanda fault. The combined findings of PSInSAR results, field observations, and geomorphic indices studies strongly suggest the presence of an active fault. When analyzing movement values, the geomorphic indices and PSInSAR methods yield higher results compared to field studies. Interestingly, the uplift and subsidence values align closely with the fault lines. Palaeoseismological studies on this fault segment will be useful. Thus, the frequency of earthquake generation can be determined approximately. The high amounts of movement obtained indicate that it has the potential to produce earthquakes. A possible earthquake will significantly affect the neighbouring provinces. The fault zone is in a position to affect several neighbouring cities.

6. Author contributions

The authors declare that they contributed to the paper in an equal way.

7. Declaration of competing interest

The authors declare that they have no known competing financial interests or personal relationships that could have appeared to influence the work reported in this paper.

8. Data availability

Data can be provided upon request.

9. Acknowledgements

As authors, we would like to thank the editor and the associate editor for their efforts. We thank reviewers who contributed to the development of the manuscript. We thank the European Space Agency (ESA) for providing SAR images (Sentinel-1).

10. References

Abdikan, S, Arıkan, M., Sanli, F.B. (2014). Monitoring of coal mining subsidence in a peri-urban area of Zonguldak city (NW Turkey) with persistent scatterer interferometry using ALOS-PALSAR. *Environ. Earth Science*, 71:4081-4089.

Arikan, M., Hooper, A., Hanssen, R. (2010). *Radar time series analysis over West Anatolia*. European Space Agency (Special Publication) ESA, SP-677.

Atabey, E. (1989). *Aksaray-H18 Quadrangle, 1:100,000 Scale Geological Map and Explanatory Text.* Ankara, Türkiye, Maden Tetkik Arama Yayınları.

Biggs, J., Wright, T., Lu, Z., Parsons, B. (2007). Multi-interferogram method for measuring interseismic deformation: Denali Fault, Alaska. *Geophysical Journal International*, 170(3), 1165-1179. doi: **https://doi.org/10.1111/j.1365-246X.2007.03415.x**

Colesenti, C., Ferretti, A., Prati, C., Rocca, F. (2001). Comparing GPS, optical levelling, and persistent scatterers. *Proceedings of IGARSS*, 2622-2624.

Çiner, A., Doğan, U., Yıldırım, C., Akçar, N., Ivy-Ochs, S., Alfimov, V., Schlüchter. C. (2015). Quaternary uplift rates of the Central Anatolian Plateau, Turkey: insights from cosmogenic isochron-burial nuclide dating of the Kızılırmak River terraces. *Quaternary Science Reviews*, 107, 81-97. doi: **https://doi.org/10.1016/j.quascirev.2014.10.007**

Demircioğlu, R. (2014). *Gülşehir-Özkonak (Nevşehir) Çevresinde Kirşehir Masifi ve Örtü Birimlerinin Jeolojisi Ve Yapisal Özellikleri.* Doktora Tezi, Selçuk Üniversitesi, Konya, Türkiye.

Demircioğlu, R. and Coşkuner, B. (2022). Salanda Fay Zonu'nun Kesikköprü (Kırşehir) ve Yeşilöz (Nevşehir) arasında kalan kesiminin göreceli tektonik aktivitesinin jeomorfik indislerle incelenmesi. *Pamukkale Üniversitesi Mühendislik Bilimleri Dergisi*, 8(3),464-482. doi: **https://dergipark.org.tr/tr/pub/pajes/issue/70618/1136992**

Doğan, U., Koçyiğit, A., Wijbrans, J. (2009). *Evolutionary history of the Kızılırmak River, Cappadocia Section: implication for the initiation of Neotectonic regime in Central Anatolia*, Turkey. 62nd Geological Congress of Turkey, Ankara, Türkiye, 13-17 Nisan.

Doğan, U. (2011). Climate-Controlled river terrace formation in the Kızılırmak Valley, Cappadocia section, Turkey: inferred from Ar-Ar dating of Quaternary basalts and terraces stratigraphy. *Geomorphology Journal*, 126, 66-81. doi: **https://doi.org/10.1016/j.geomorph.2010.10.028**

Dumka, R. K., SuriBabu, D., Malik, K., Prajapati, S. and Narain, P. (2020). PS-InSAR derived deformation study in the Kachchh, Western India. *Applied Computing and Geosciences*, 8, 100041. doi: **https://doi.org/10.1016/j.acags.2020.100041**

Dumka, R. K., Suribabu, D., Narain, P., Kothyari, G. C., Taloor, A. K. and Prajapati, S. (2021). PSInSAR and GNSS derived deformation study in the West part of Narmada Son Lineament (NSL), western India. *Quaternary Science Advances*, 4, 100035.

Dumka, R. K., Suribabu, D. and Prajapati, S. (2022). PSI and GNSS derived ground subsidence detection in the UNESCO Heritage City of Ahmedabad, Western India. *Geocarto International*, 37, 25, 7639-7658. doi: **https://doi.org/10.1080/10106049.2021.1980618**

Suribabu, D., Dumka, R. K., Paikray, J., Kothyari, G. C., Thakkar, M., Swamy, K. V., Taloor, A. K. and Prajapati, S. (2022). Geodetic characterization of active Katrol Hill Fault (KHF) of Central Mainland Kachchh, western India. *Geodesy and Geodynamics*, 13, 247-253. doi: **https://doi.org/10.1016/j.geog.2021.05.003**

Suribabu, D., Dumka, R. K., Kothyari, G. C., Swamy K. V. and Prajapati, S. (2022c). Identification of crustal deformation in the Saurashtra region, western India: insights from PSI and GNSS derived investigation. *Acta Geodaetica et Geophysica*, 57, 639-659. doi: **https://doi.org/10.1007/s40328-022-00399-z**

Dumka, R. K., Prajapati, S., SuriBabu, D., Swamy, K. V., Kothyyari, G. C. and Malik, K. (2023). GPS and InSAR derived evidences of intra-basin stress and strike-slip tectonics in the vicinity of 2001 (M7.7) earthquake, Kachchh, western India. *Geological Journal*, 58, 683-699. doi: **https://doi.org/10.1002/gj.4618**

Emre, Ö., Duman, T.Y., Özalp, S., Elmacı, H., Olgun, Ş., Şaroğlu, F. (2013). *Açıklamalı Türkiye Diri Fay Haritası Ölçek 1/1.125.000:* Maden Tetkik ve Arama Genel Müdürlüğü Özel Yayın Serisi 30. ISBN: 978605531056.

Famiglietti, N.A., Golshadi, Z., Vallianatos, F., Caputo, R.; Kouli, M., Sakkas, V., Atzori, S., Moschillo, R., Cecere, G., D'Ambrosio, C. *et al.* (2021). Greece Central Crete ML 5.8 Earthquake: An Example of Coalescent Fault Segments Reconstructed from InSAR and GNSS Data. *Remote Sensing, 14*, 5783. **https://doi.org/10.3390/rs14225783**

Ferretti, A., Prati, C. and Rocca, F. (2001). Permanent scatterers in SAR interferometry. *IEEE Transactions on Geoscience and Remote Sensing*, 39, 8-20. doi: **http://dx.doi.org/10.1109/36.898661**

Gezgin, C. (2022). Using the PS-InSAR technique, the influence of groundwater levels on land subsidence in Karaman (Turkey). *Advances in Space Research, 70*, 3568-3581. doi: **https://doi.org/10.1016/j.asr.2022.08.003**

Gündüz, H. İ., Yılmaztürk, F. and Orhan, O. (2023). An Investigation of Volcanic Ground Deformation Using InSAR Observations at Tendürek Volcano (Turkey). *Applied Sciences*, 13, 6787. doi: **https://doi.org/10.3390/app13116787**

Gürsoy, Ö., Kaya, Ş., Çakir, Z., Tatar, O., Canbaz, O. (2017). Determining lateral offsets of rocks along the eastern part of the North Anatolian Fault Zone (Turkey) using the spectral classification of satellite images and field measurements. *Geomatics, Natural Hazards, and Risk*, 8(2), 1276-1288. doi: **https://doi.org/10.1080/19475705.2017.1318794**

Hastaoğlu, K.Ö., Poyraz, F., Türk, T., Koçbulut, F., Şanlı, U., Yılmaz, I., Şanlı, F.B., Kuçak, R.A., Demirel, M., Gürsoy, Ö., and Duman, H. (2015). GPS ve PS-InSAR yöntemleri kullanılarak Koyulhisar (Sivas) heyelanlarının izlenmesi: ilk sonuçlar. *Gümüşhane Üniversitesi Fen Bilimleri Enstitüsü Dergisi*, 4, 2, 161-175. doi: **https://doi.org/10.17714/gufbed.2014.04.013**

He, P., Wen, Y., Xu, C., Chen, Y. (2018). High-quality three-dimensional displacement fields from new-generation SAR imagery: application to the 2017 Ezgeleh, Iran, earthquake. *Journal of Geodesy*, 93. doi: **https://doi.org/10.1007/s00190-018-1183-6**

Hooper, A., Zebker, H., Segall, P., Kampes, B. (2004). A new method for measuring deformation on volcanoes and other natural terrains using InSAR persistent scatterers. *Geophysical Research Letters*, 31(23):5. doi: **https://doi.org/10.1029/2004GL021737**

Hooper, A, Segall, P, Zebker, H. (2007). Persistent Scatterer InSAR for crustal deformation analysis with application to Volcán Alcedo. *Galápagos Journal of Geophysical Research*, 112: B07407. doi: **https://doi.org/10.1029/2006JB004763**

Hooper, A., Bekaert, D., Hussain, E., and Spaans, K. (2018). *Stamps/Manual, VeStamps4.1b*, School of Environment, University of Leeds, LS2 9JT Leeds, UK.

Howell, A., Nissen, E., Stahl, T., Clark, K., Kearse, J., Van Dissen, R., Jones, K. (2020). Three-dimensional surface displacements during the 2016 MW 7.8 Kaikōura earthquake (New Zealand) from photogrammetry-derived point clouds. *Journal of Geophysical Research: Solid Earth*, 125(1), e2019JB018739. doi: **https://doi.org/10.1029/2019JB018739**

Kandıllı. (2022). *Observatory Regıonal Earthquake-Tsunami Monıtorıng And Evaluatıon Centre*. 18 January 2022 Sarıoglan-Kayserı Earthquake. Press Release.

Koçyiğit, A. (2003). Orta Anadolu'nun genel neotektonik özellikleri ve depremselliği. *Türkiye Petrol Jeologları Derneği Bülteni*, 5(Özel Sayı), 1-26.

Koçyiğit, A., Doğan, U. (2016). The strike-slip neotectonic regime and related structures in the Cappadocia region: a case study in the Salanda basin, Central Anatolia, *Turkey. Turkish Journal of Earth Sciences*, 25(5), 393-417. doi: **https://doi.org/10.3906/yer-1512-9**

Liu, J., and Zhao, X. (2020). GNSS Fault Detection and Exclusion Based on Virtual Pseudorange-Based Consistency Check Method. *Chinese Journal of Electronics*, 29(1), 41-48. doi: **https://doi.org/10.3390/s20030590**

Lu, P., Han, J., Hao, T., Li, R. and Qiao, G. (2020). Seasonal deformation of permafrost inWudaoliang basin in Qinghai-Tibet plateau revealed by StaMPS-InSAR. *Marine Geodesy*, 43, 248-268. doi: **https://api.semanticscholar.org/CorpusID:213881589**

Meisina, C., Zucca, F., Fossati, D., Ceriani, M., Allievi, J. (2006). Ground deformation monitoring by using the permanent scatterers technique: the example of the Oltrepo Pavese (Lombardia, Italy, *Engineering Geology*, 88(3-4):240-259.

Oktar, O., Erdoğan, H., Poyraz, F., and Tiryakioğlu, İ. (2021). Investigation of deformations with the GNSS and PSInSAR methods. *Arabian Journal of Geosciences*, 14, 2586. doi: **https://doi.org/10.1007/s12517-021-08765-x**

Florian, P., Heidrun, K., Dietrich, L., Katrin, H., Morelia, U. (2019). Measuring tectonic seafloor deformation and strain-build up with acoustic direct-path ranging, *Journal of Geodynamics*, 124, 14-24. doi: **https://doi.org/10.1016/j.jog.2019.01.002**

Peyret, M., Rolandone, F., Dominguez, S., Djamour, Y., Meyer, B. (2008). Source model for the Mw 6.1, 31 March 2006, Chalan-Chulan earthquake (Iran) from InSAR. *Terra Nova* 20(2):126-133. doi: **https://doi.org/10.1111/j.1365-3121.2008.00797.x**

Poyraz, F., Hastaoğlu, K.Ö. (2020). Monitoring of tectonic movements of the Gediz Graben by the PSInSAR method and validation with GNSS results. *Arabian Journal of Geosciences*, 13:844. doi: **https://doi.org/10.1007/s12517-020-05834-5**

Rodríguez, R., Lira, J., & Rodríguez, I. (2012). Subsidence risk due to groundwater extraction in urban areas using fractal analysis of satellite images. *Geofísica Internacional*, 51(2),157–167. doi: **https://doi.org/10.22201/igeof.00167169p.2012.51.2.605**

Rosu, A.M., Pierrot-Deseilligny, M., Delorme, A., Binet, R., Klinger, Y. (2015). Measurement of ground displacement from optical satellite image correlation using the free open-source software MicMac. *ISPRS Journal of Photogrammetry and Remote Sensing*, 100, 48-59. doi: **https://doi.org/10.1016/j.isprsjprs.2014.03.002**

Scott, C., Bunds, M., Shirzaei, M., Toke, N. (2020). Creep along the Central San Andreas Fault from surface fractures, topographic differencing, and InSAR. *Journal of Geophysical Research: Solid Earth, 125*, e2020JB019762. doi: **https://doi.org/10.1029/2020JB019762**

Shirzaei, M., and Bürgmann, R. (2013). Time-dependent model of creep on the Hayward fault from joint inversion of 18 years of InSAR and surface creep data. *Journal of Geophysical Research: Solid Earth*, 118(4), 1733-1746. doi: **https://doi.org/10.1002/jgrb.50149**

Suárez, G. ., Jaramillo, S. H., López-Quiroz, P., & Sánchez-Zamora, O. (2018). Estimation of ground subsidence in the city of Morelia, Mexico using Satellite Interferometry (INSAR)s. *Geofísica Internacional*, 57(1), 39-58. doi: **https://doi.org/10.22201/igeof.00167169p.2018.57.1.1821**

Şaroğlu, F., Emre, Ö., Aydoğan, B. (1987). Türkiye'nin diri fayları ve depremsellikleri. Maden Tetkik ve Arama Genel Müdürlüğü, Ankara, Türkiye, 394.

Şengör, A.M.C., Yılmaz, Y. (1981). Tethyan evolution of Turkey: a plate tectonic approach. *Tectonophysics*, 75(3-4), 181-241. doi: **https://doi.org/10.1016/0040-1951(81)90275-4**

Temiz, U. (2004). Kırşehir Dolayının Neotektoniği ve Depremselliği. PhD, Ankara University, Ankara, Turkey.

Temiz, U., Gökten, E., Eikenberg, J. (2009). U/Th dating of fissure

ridge travertines from the Kırşehir region (Central Anatolia Turkey): structural relations and implications for the Neotectonic development of the Anatolian block. *Geodin Acta 22*: 201-213. doi: **https://doi.org/10.3166/ga.22.201-213**

Wang, T., and Jónsson, S. (2015). Improved SAR amplitude image offset measurements for deriving three-dimensional coseismic displacements. *IEEE Journal of Selected Topics in Applied Earth Observations and Remote Sensing*, 8 (7), 3271-3278. doi: **https://doi.org/10.1109/JSTARS.2014.2387865**

Yavaşoğlu, H., Tarı, E., Tüysüz, O., Çakır, Z., Ergintav, S. (2011). Determining and modelling tectonic movements along the central part of the North Anatolian Fault (Turkey) using geodetic measurements. *Journal of Geodynamics*, 51(5), 339-343. doi: **https://doi.org/10.1016/j.jog.2010.07.003**

Yen, J.Y., Lu, C.H., Chang, C.P., Hooper, A., Chang, Y.H., Liang, W.T., Chang, T.Y., Lin, M.S., Chen, K.S. (2011). Investigating active deformation in the northern longitudinal valley and City of Hualien in Eastern Taiwan using persistent scatterer and small-baseline SAR interferometry. *Terrestrial Atmospheric and Oceanic Sciences*, 22(3):291-304. doi: **https://scihub.copernicus.eu/dhus/#/home**